Regenerative Therapy 26 (2024) 850–858

Contents lists available at ScienceDirect

Regenerative Therapy

journal homepage: http://www.elsevier.com/locate/reth

Original Article

Osteogenic effects and safety of human induced pluripotent stem cell-derived megakaryocytes and platelets produced on a clinical scale

Takahito Arai [a], Yasuhiro Shiga [a, *], Michiaki Mukai [a], Naoya Takayama [b], Susumu Tashiro [a], Ikuko Tajiri [a], Kentaro Kosaka [c], Masashi Sato [d], Sou Nakamura [e], Haruki Okamoto [e], Seiji Kimura [a], Kazuhide Inage [a], Miyako Suzuki-Narita [f], Yawara Eguchi [a], Sumihisa Orita [g], Koji Eto [b, e], Seiji Ohtori [a]

[a] Department of Orthopaedic Surgery, Chiba University Graduate School of Medicine, Chiba, 2608670, Japan
[b] Department of Regenerative Medicine, Chiba University Graduate School of Medicine, Chiba, 2608670, Japan
[c] Department of Plastic, Reconstructive, and Aesthetic Surgery, Graduate School of Medicine, Chiba University, Chiba, 2608670, Japan
[d] Department of Orthopaedic Surgery, Eastern Chiba Medical Center, Chiba, 2838686, Japan
[e] Department of Clinical Application, Center for IPS Cell Research and Application (CiRA), Kyoto University, Kyoto, 6068507, Japan
[f] Department of Bioenvironmental Medicine, Graduate School of Medicine, Chiba University, Chiba, 2608670, Japan
[g] Center for Frontier Medical Engineering, Chiba University, Chiba, 2638522, Japan

ARTICLE INFO

Article history:
Received 25 July 2024
Received in revised form
16 September 2024
Accepted 25 September 2024

Keywords:
Platelet-rich plasma
Freeze-dried human induced pluripotent stem cell-derived megakaryocytes and platelets
VerMES incubator
Osteogenesis
Lumber spine

ABSTRACT

Introduction: Platelet-rich plasma obtained by centrifuging peripheral blood can promote osteogenesis owing to its abundant growth factors but has drawbacks, including rapid growth factor loss and inconsistent effects depending on donor factors. To overcome these issues, we were the first in the world to use freeze-dried human induced pluripotent stem cell-derived megakaryocytes and platelets (S-FD-iMPs) and found that they have osteogenesis-promoting effects. Since turbulence was found to activate platelet biogenesis and iPS cell-derived platelets can now be produced on a clinical scale by a device called VerMES, this study examined the osteogenesis-promoting effect and safety of clinical-scale FD-iMP (V-FD-iMPs) for future human clinical application.

Method: We administered either S-FD-iMPs, V-FD-iMPs, or saline along with artificial bone to the lumbar spine of 8-week-old male Sprague–Dawley rats (n = 4 each) and evaluated bone formation by computed tomography (CT) and pathology. Next, we administered V-FD-iMPs or saline along with artificial bone to the lumber spines of 5-week-old male New Zealand White rabbits (n = 4 each) and evaluated the bone formation by CT and pathology. Rats (n = 10) and rabbits (n = 6) that received artificial bone and V-FD-iMPs in the lumbar spine were also observed for 6 months for adverse events, including infection, tumor formation, and death.

Results: Both V-FD-iMPs and S-FD-iMPs significantly enhanced osteogenesis in the lumber spines of rats in comparison with the controls 8 weeks postoperatively, with no significant differences between them. Furthermore, V-FD-iMPs vigorously promoted osteogenesis in the lumber spines of rabbits 8 weeks postoperatively. In rats and rabbits, V-FD-iMPs showed no adverse effects, including infection, tumor formation, and death, over 6 months.

Conclusion: These results suggest that V-FD-iMPs promote safe osteogenesis.

Abbreviations: bFGF, basic fibroblast growth factor; BV/TV, bone volume/tissue volume; CT, computed tomography; Dox, doxycycline; S-FD-iMPs, FD-iMPs produced with a shaker incubator; V-FD-iMPs, FD-iMPs produced with a VerMES incubator; FD-iMPs, freeze-dried human induced pluripotent stem cell-derived megakaryocytes and platelets; HE, hematoxylin-eosin; hiPSCs, human induced pluripotent stem cells; imMKCLs, immortalized megakaryocyte cell lines; iMPs, megakaryocytes and platelets; PDGF, platelet-derived growth factor; PRP, platelet-rich plasma; rabbit-C group, rabbit control group; rabbit-S group, rabbit shaker group; rabbit-V group, rabbits VerMES group; rat-C group, rat control group; rat-S group, rat shaker group; rat-V group, rat VerMES group; SCF, stem cell factor; Tb.N, trabecular branch number; Tb.Sp, trabecular separation; Tb.Th, trabecular thickness; TGF, transforming growth factor.

* Corresponding author. Department of Orthopaedic Surgery, Chiba University Graduate School of Medicine, 1-8-1, Inohana, Chuo-ku, Chiba-shi, Chiba, Japan.
E-mail address: yshiga1111@yahoo.co.jp (Y. Shiga).

Peer review under responsibility of the Japanese Society for Regenerative Medicine.

https://doi.org/10.1016/j.reth.2024.09.012

1. Introduction

Platelets, abundant in various growth factors, are critical components of platelet-rich plasma (PRP) generated from peripheral blood. PRP is often used for the treatment of knee osteoarthritis, rotator cuff injuries, lateral epicondylitis, and Achilles tendonitis [1–4]. It reportedly promoted bone formation and fusion [5–7] and is expected to be effective for spinal fusion surgery, which requires early bone fusion.

However, PRP use has some limitations. The major limitation is that the effectiveness of PRP remains to be established. Some researchers have reported that PRP promotes bone fusion without immunoreaction or infection [5,8–11], whereas others have reported no positive effect on bone fusion [12–14]. These discrepancies may be due to the heterogeneous quality of PRP derived from patient blood. The amount of growth factors is variable and depends on donor characteristics, such as age, sex, and platelet count [15], as well as collection and processing protocols.

Another disadvantage is that the growth factors in PRP are unstable and lost within a few days [16]. Thus, PRP should be administered clinically as soon as it is prepared; however, this approach requires blood sampling just before surgery, along with installation of centrifugal separators at each facility, imposing physical and financial burden on patients and healthcare institutions.

To overcome these issues, we previously validated platelets derived from human induced pluripotent stem cells (hiPSCs) for bone regeneration. We established a method to produce a large number of platelets using immortalized megakaryocyte cell lines (imMKCLs) derived from hiPSCs [17–19]. We also addressed the shelf-life limitations of platelets through freeze-drying technology; we found that freeze-dried PRP stably maintains cytokine levels during sealed storage for more than 1 month at room temperature and promotes bone formation in animals, similar to fresh PRP [20,21].

By integrating these technologies, we developed freeze-dried megakaryocytes and platelets derived from human induced pluripotent stem cells (FD-iMPs). FD-iMPs can be prepared as a powder and dissolved in saline before use. In a previous study, we found that FD-iMPs promoted bone formation on a rat lumbar spine using artificial bone as a carrier [22]. However, FD-iMPs used in the previous experiments were produced on a small experimental scale in a shaking incubator called a “shaker,” and the number of platelets was insufficient for human clinical applications. Recently, we found that turbulence plays an essential role in platelet release from megakaryocytes and established a unique technique for generating large quantities (in the order of 100 billion; approximately 100 times the number that can be produced at one time using a shaker) of platelets derived from imMKCLs using a device called “VerMES” [23]. Moreover, a subsequent study demonstrated that the platelets produced using this method could be safely transfused into humans for clinical scenarios [24,25]. Therefore, we attempted to validate whether VerMES-generated FD-iMPs (V-FD-iMPs) promote bone formation as well as shaker-generated FD-iMPs (S-FD-iMPs) in rat and rabbit lumbar spines without causing adverse events, such as infection, tumor formation, and death.

2. Methods

2.1. Animals

All animal experiments were approved by the Ethics Committee of Chiba University. All experiments were conducted in accordance with the National Institutes of Health Guidelines for the Management and Use of Laboratory Animals, and this study was conducted in accordance with the ARRIVE guidelines. Eight-week-old male Sprague–Dawley rats (n = 32; weighing 250–300 g) (CLEA, Tokyo, Japan) and 5-week-old male New Zealand White rabbits (n = 20; weighing 0.7–1.0 kg) (CLEA, Tokyo, Japan) were used in this study. The animals were kept under a 12-:12-h light/dark cycle at 21°C-23 °C and 45%–65 % humidity. All the animals were provided water and a standard diet (Oriental Yeast Co., Ltd., Tokyo, Japan).

2.2. Production of iMPs

2.2.1. Cell culture and reagents

Similar to a previous study [22], we cultured imMKCLs (MKCL line 7) [17] in 500 mL of Iscove's modified Dulbecco medium (Sigma-Aldrich, St. Louis, MO, USA) containing 90 mL of fetal bovine serum (10270–106; Thermo Fisher Scientific, Waltham, MA, USA); 600 μL of L-ascorbic acid (A4544; Sigma-Aldrich); 600 μL of 1-thioglycerol (M6145; Sigma- Aldrich); 6 mL of a cocktail of 12000 units/mL penicillin, 10000 mcg/mL of streptomycin, and 200 mM L-glutamine (10378–016; Thermo Fisher Scientific); 6 mL of a cocktail of 1 mg/mL human insulin, 0.55 mg/mL human transferrin, and 0.67 μg/mL sodium selenite (41400–045; Thermo Fisher Scientific) in the presence of 50 ng/mL human stem cell factor (SCF; 193–15513; Wako, Tokyo, Japan), 200 ng/mL TA316 (human thrombopoietin mimetic small compound, in-house synthesized) [23], and 100 μg/mL doxycycline (Dox; Clontech, Mountain View, CA, USA).

2.2.2. Preparation of S-FD-iMPs from hiPSCs

To produce platelets from imMKCLs, a Dox-off medium was prepared by excluding Dox from the medium mentioned above and adding 750 μM SR1 (aryl hydrocarbon receptor antagonist; NARD Institute, Hyogo, Japan), 10 mM Y27632 (Rho-associated protein kinase inhibitor; Wako Pure Chemicals, Osaka, Japan), and 15 mM KP457 (inhibitor of GPIbα shedding on platelets; Kaken Pharmaceutical, Tokyo, Japan). The medium and megakaryocytes were placed in 125-mL Erlenmeyer cell culture flasks at 1.0×10^5 cells/mL each and incubated in Lab-Therm shakers (Kuhner, Basel, Switzerland) at 37 °C under 5 % CO_2. After incubating for 5 d, the contents of all flask cultures were combined and centrifuged at 700×*g* for 15 min to collect the mixed product of megakaryocytes and platelets (iMPs).

The cell pellet was suspended in phosphate-buffered saline (0.5 mL per flask/2 % of the volume of the culture medium), followed by the addition of 1 M $CaCl_2$ (10 μL/flask) and 10000 U/mL thrombin (10 μL/flask) and incubation at 37 °C for 1 h for activation.

The platelet solution was divided into test tubes (1 mL each), frozen at −60 °C for 24 h, and freeze-dried to powder form. The powder was dissolved in 1 mL of saline solution and used for the experiment as S-FD-iMPs (Fig. 1a).

2.2.3. Preparation of V-FD-iMPs from hiPSCs

VerMES can efficiently produce platelets on a large scale by generating turbulence, which is vital for platelet release from megakaryocytes. Using the same imMKCL strain as that used for preparing S-FD-iMPs, we cultured the cells at a concentration of 1.0 × 105 cells/mL for 5 d in 2.4 L of Dox-off medium with the same composition as that used for preparing S-FD-iMPs with VerMES (Fig. 1b). The harvested mixture of megakaryocytes and platelets was activated using a procedure similar to that used for S-FD-iMPs. Subsequently, the solution was divided into 1 mL portions and freeze-dried, and the powder was dissolved in 1 mL of the saline solution immediately before use (Fig. 1c).

2.3. Measurement of growth factors in iMPs

The expression levels of growth factors, including transforming growth factor (TGF)-β, platelet-derived growth factor (PDGF)-BB, and basic fibroblast growth factor (bFGF), were quantified using enzyme-linked immunosorbent assay kits (Quantikine®; R&D Systems, Minneapolis, MN, USA). Each preparation was dissolved in 1 mL saline solution and used for the cytokine assays. S-FD-iMPs were tested three times as biological triplicates and V-FD-iMPs were tested twice as biological duplicates. Each test of V-FD-iMPs included two technical replicates, resulting in a total of four measurements. In contrast, S-FD-iMPs had a total of three measurements. All assays were performed following the manufacturer's instructions. All growth factor levels were analyzed immediately after freeze-drying.

2.4. Experiments with rats

2.4.1. Artificial bone grafting to rat lumbar spine

Based on previous studies [22,26], all rats were anesthetized abdominally with an anesthetic mixture consisting of 2.5 mg/kg butorphanol (Meiji Seika Pharma. Co., Ltd., Tokyo, Japan), 0.15 mg/kg medetomidine (Nippon Zenyaku Kogyo Co., Ltd., Koriyama, Japan), 2.0 mg/kg midazolam (Maruishi Pharmaceutical Co., Ltd., Osaka, Japan), and 1.45 mL/kg of saline (Otsuka Pharmaceutical Co., Ltd., Tokyo, Japan).

The rats were randomly divided into three groups and subjected to surgical procedures. We shaved the backs of the rats, incised the skin and fascia, and detached the muscles from the L4-6 spinous processes to the transverse processes without decortication. Each group was administered the following materials on the lumbar spine, and the fascia and skin of the rats were sutured:

Control group (rat-C group): 1 mL of saline and artificial bone (n = 14).

Shaker group (rat-S group): 1 mL of S-FD-iMPs and artificial bone (n = 4).

VerMES group (rat-V group): 1 mL of V-FD-iMPs and artificial bone (n = 14).

The artificial bone was 1 cm^3 of a composite of hydroxyapatite and collagen (Refit©: HOYA Technosurgical Corporation, Tokyo, Japan) (Fig. 1d).

2.4.2. Radiographic evaluation of the rats

Bone formation over time was monitored in four rats from each group, which underwent computed tomography (CT) preoperatively and 2, 4, 6, and 8 weeks postoperatively. Five consecutive axial spine images were selected to analyze bone formation between the L5 and L6 vertebrae at each time point, and their cross-sectional areas were calculated using the ImageJ software (NIH, Bethesda, MD, USA). By averaging five slices per time point, we computed the ratio of preoperative to postoperative values for each rat. This normalization accounted for individual body size variations (Fig. 1e). The mean values for each group were compared.

2.4.3. Histopathological evaluation of the rats

After obtaining CT scans 8 weeks postoperatively, only the rats involved in the radiological evaluation were euthanized. Two rats were randomly selected from the rat-C and rat-V groups, and their vertebrae were harvested. These vertebral bodies were subjected to demineralization using U·I demineralization solution A (#0005810; U·I Kasei, Amagasaki, Japan) for 3 d, followed by neutralization with 5 % sodium sulfate overnight.

The L5 vertebral body was dissected, and the sections were processed into paraffin blocks using a dehydration permeation machine (Tissue-Tek V.I.P 6 AI; Sakura Finetech Japan Co., Ltd., Tokyo, Japan). The paraffin used was Parabet 60 GR (#43257; Muto Pure Chemicals Co., Ltd., Tokyo, Japan), which melts at 58°C-60 °C. Thin sections (thickness, approximately 4–5 μm) were cut from the paraffin blocks using a sliding microtome (LS113; YAMATO-KOHKI Industrial Co., Ltd., Asaka, Japan). These tissue slices were applied to glass slides (#5116; Muto Pure Chemicals) coated with 3-aminopropyltrimethoxysilane (APS). After drying overnight, the sections were stained with hematoxylin-eosin (HE). The structure of the trabecular bone in the newly formed area was observed under a microscope (Fig. 1f).

2.4.4. Long-term safety study of V-FD-iMPs in rats

Ten rats each from the rat-C and rat-V groups, which were not used for radiological evaluation, were maintained for 6 months. While CT scans of the lumbar spine were obtained monthly, all rats were also observed for adverse events such as infection, tumor formation, and death.

2.5. Experiments with rabbits

2.5.1. Artificial bone grafting to rabbit lumbar spine

Following the literature, all rabbits were anesthetized using intramuscular injection of an anesthetic mixture of medetomidine 0.15 mg/kg, midazolam 1.0 mg/kg, and butorphanol 1.5 mg/kg [27].

All rabbits were randomly divided into two groups and treated with reference to previous studies [28–30]. The rabbits' backs were shaved, and 5 cm incisions were made along the midline. Only the fasciae to the right of the L6-7 spinous processes were incised, and the muscles were detached from the spinous and transverse processes without decortication, as in the rats. No procedures were performed on the left side. The following materials were administered to the right vertebral arch and transverse processes of rabbits in each group; the fascia and skin were then sutured.

Control group (rabbit-C group): 1 mL of saline and artificial bone (n = 10).

VerMES group (rabbit-V group): 1 mL of V-FD-iMPs and artificial bone (n = 10).

As in the rats, 1 cm^3 of Refit©, a composite of hydroxyapatite and collagen, was used as the artificial bone (Fig. 1d).

2.5.2. Radiographic evaluation of the rabbits

We selected four rabbits from each group and observed bone formation in their vertebrae over time. CT was undertaken preoperatively and every 2 weeks postoperatively until 8 weeks. In each of five consecutive axial images between the L6 and L7 vertebrae, the vertebral body was divided in the midline, and the areas of the right and left sides were measured using the ImageJ software [22]. The ratio of the area on the right side with the implanted artificial bone to the left side without intervention was calculated and averaged. The mean values for each group were calculated and compared.

2.5.3. Histopathological evaluation of the rabbits

After CT scans for 8 weeks postoperatively, all rabbits involved in the radiological evaluation were euthanized. Three rabbits were randomly selected from each group, and their lumbar vertebral bodies were extracted. As in the rats, axial sections of L6 vertebrae were HE stained. The structure of the trabecular bone in the newly formed area was observed under a microscope.

The bone trabeculae showing new bone formation from the right transverse process to the spinous process were measured using the Histometry RT digitizer (System Supply, Ina, Japan) to determine (1) trabecular bone area (bone volume/tissue volume [BV/TV], %), (2) trabecular branch number (Tb.N, N/mm), (3) trabecular thickness (Tb.Th, μm), and (4) trabecular separation (Tb.Sp, μm) [31,32].

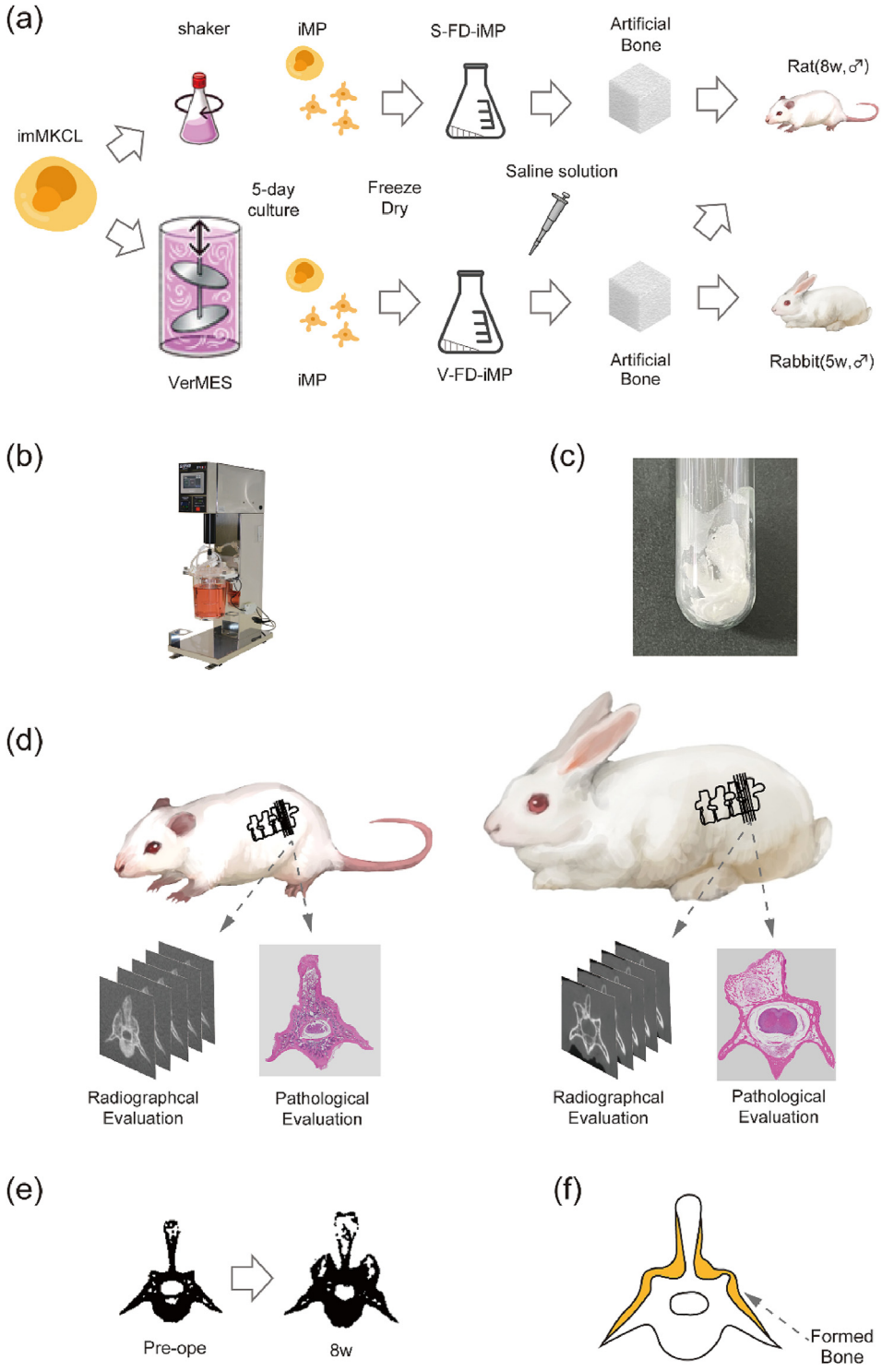

Fig. 1. Flow of this experiment and the evaluation method
(a) iMPs fabrication method and animal experiment flow. The megakaryocytes were cultured and differentiated for 5 d using a shaker or VerMES, freeze-dried, dissolved in saline solution, and implanted into the lumbar vertebrae of the animals along with the artificial bone. (b) Photograph of VerMES. (c) Photograph of freeze-dried iPS cell-derived platelet product. (d) Evaluation methods for the animal experiments. At each time point, computed tomography (CT) scans of the lumbar spine were obtained for radiological evaluation. After euthanasia, the vertebrae were pathologically evaluated. (e) Evaluation of the rat CT scans. On the left is a preoperative CT cross-sectional image and on the right is an image of the same location 8 weeks after surgery. As shown in this example, both images were processed using the ImageJ software, and the preoperative and postoperative area ratios were calculated. (f) Schematic representation of the pathological evaluation method. We evaluated the structure of the newly formed bone (area highlighted in orange) at the artificial bone graft site.

2.5.4. Long-term safety evaluation of V-FD-iMPs in rabbits

As with the rats, six rabbits in each group that were not used for radiological evaluation were maintained for 6 months. They were followed up monthly with CT and observed for adverse events.

2.6. Statistical analysis

The rat bone formation results were compared among three groups using Tukey's test. The other results of the rabbit and in vitro experiments were evaluated using Student's *t*-tests in two-group comparisons. Differences were considered statistically significant at $P < 0.05$. For the long-term safety study, Kaplan–Meier survival curves were drawn for the occurrence of adverse events.

3. Results

3.1. Quantification of growth factors

Initially, we measured the growth factors in the clinical-scale V-FD-iMPs and experimental-scale S-FD-iMPs using enzyme-linked immunosorbent assay. S-FD-iMPs contained 9.3 ± 1.8 ng/mL PDGF-BB, 53.7 ± 3.8 ng/mL TGF-β, and 25.4 ± 3.1 ng/mL bFGF, whereas V-FD-iMPs contained 1.4 ± 0.1 ng/mL PDGF-BB, 167.4 ± 3.6 ng/mL TGF-β, and 38.9 ± 0.8 ng/mL bFGF.

3.2. Radiographic evaluation of rats

We administered V-FD-iMPs (rat-V group), S-FD-iMPs (rat-S group), or saline (rat-C group) along with artificial bone to the lumbar spines of rats and compared the amount of new bone formation over time using CT. CT images showed that bone formation increased over time in all groups. More vigorous bone formation was observed in the rat-V and rat-S groups than in the rat-C group (Fig. 2a). At 4, 6, and 8 weeks after surgery, bone formation was significantly greater in the rat-V and rat-S groups than in the rat-C group. Bone formation in the rat-V group was not less than that in the rat-S group (Fig. 2b).

3.3. Histopathological evaluation of rats

Eight weeks postoperatively, the areas of newly formed bone in the rat-C and rat-V groups were examined microscopically (Fig. 2c). In both groups, new bone formed on the vertebral arch and the transverse process, where the artificial bone was implanted. The boundary with the internal bone tissue was indistinct, suggesting that remodeling had occurred.

3.4. Long-term safety study in rats

During the 6-month observation period, the rat-C and rat-V groups showed no adverse events, such as infection, tumor formation, and death (Fig. 2d).

3.5. Radiographic evaluation of rabbits

We then administered V-FD-iMPs (rabbit-V group) or saline (rabbit-C group) along with artificial bone to the right side of the lumbar vertebrae of rabbits and compared the amount of new bone formation. On the CT images, more vigorous bone formation was observed on the right than on the left side in the rabbit-V group (Fig. 3a). At 4, 6, and 8 weeks after surgery, the rabbit-V group had a significantly higher right/left bone volume ratio than the rabbit-C group (Fig. 3b).

3.6. Histopathological evaluation of rabbits

We compared the pathology of the newly formed bone trabeculae of the rabbit-V and rabbit-C groups at 8 weeks postoperatively. In the rabbit-V group, trabecular bone branches appeared to be formed finely and abundantly (Fig. 3c). Furthermore, the pathological images were quantitatively evaluated based on four parameters: (1) BV/TV (%), (2) Tb.N (N/mm), (3) Tb.Th (μm), and (4) Tb.Sp (μm). In the rabbit-V group, BV/TV and Tb.N were significantly larger, and Tb.Sp was significantly smaller than those in the rabbit-C group. Thus, while the width of the trabecular bone was almost the same in both groups, the number of beams was greater and the trabecular bone was denser in the rabbit-V group than in the rabbit-C group (Fig. 3d).

3.7. Long-term safety study in rabbits

During the 6-month observation period, no adverse events were observed in the rabbit-C and rabbit-V groups (Fig. 3e).

4. Discussion

To our knowledge, this is the first study to examine the osteogenic effects of iPS cell-derived platelets produced on a clinical scale. Recently, we found that turbulence is crucial for releasing platelets from megakaryocytes. The development of VerMES, which recapitulates this turbulence in vitro, has made it possible to produce platelets in sufficient numbers for clinical use. Platelets produced via imMKCL derived from hiPSCs are larger than normal platelets, but their functions are comparable. They have been transfused in clinical trials with no adverse effects [23,24]. Our previous studies have shown that S-FD-iMPs contain various growth factors, mainly TGF-β and PDGF-BB [22], and that they promote bone formation when administered with artificial bone to rat spines.

In this study, we compared the osteogenic potential of FD-iMPs produced at a clinical scale (V-FD-iMPs) with that of FD-iMPs produced at a laboratory scale (S-FD-iMPs). In addition, we investigated the long-term safety of the V-FD-iMP preparations. First, we examined the difference between V-FD-iMPs and S-FD-iMPs. Both V-FD-iMPs and S-FD-iMPs contained comparable levels of major cytokines. We then examined the osteogenic potential of both preparations and found that they significantly promoted more bone formation than the control group and had comparable effects. These results suggest that both preparations contain enough growth factors for *in vivo* bone formation. In addition, the rat-V and rat-C groups showed no adverse effects such as infection, tumor formation, and death, for at least 6 months. Therefore, we concluded that V-FD-iMPs promote bone formation as well as S-FD-iMPs without any adverse effects. Second, we examined the osteogenic effects and long-term safety of the V-FD-iMP preparation in medium-sized animals in anticipation of future clinical trials. We found that V-FD-iMPs promoted bone formation in a rabbit lumbar spine without causing adverse effects. We also discovered that V-FD-iMPs promoted higher density and better-quality bone formation in the same model in a quantitative pathological evaluation. These experiments showed that V-FD-iMPs also have a favorable osteogenesis-promoting effect.

Here, we discuss the mechanism by which iMP preparations promote bone formation. PRP has been reported to stimulate bone formation, and the mechanism is thought to involve multiple cytokines such as PDGF, TGF-β, and insulin growth factor. Although simple comparisons are difficult because PRP preparation methods and platelet volume vary among studies, it has been reported that PRP contains approximately 3 ng/mL PDGF, 15 ng/mL TGF-β, and

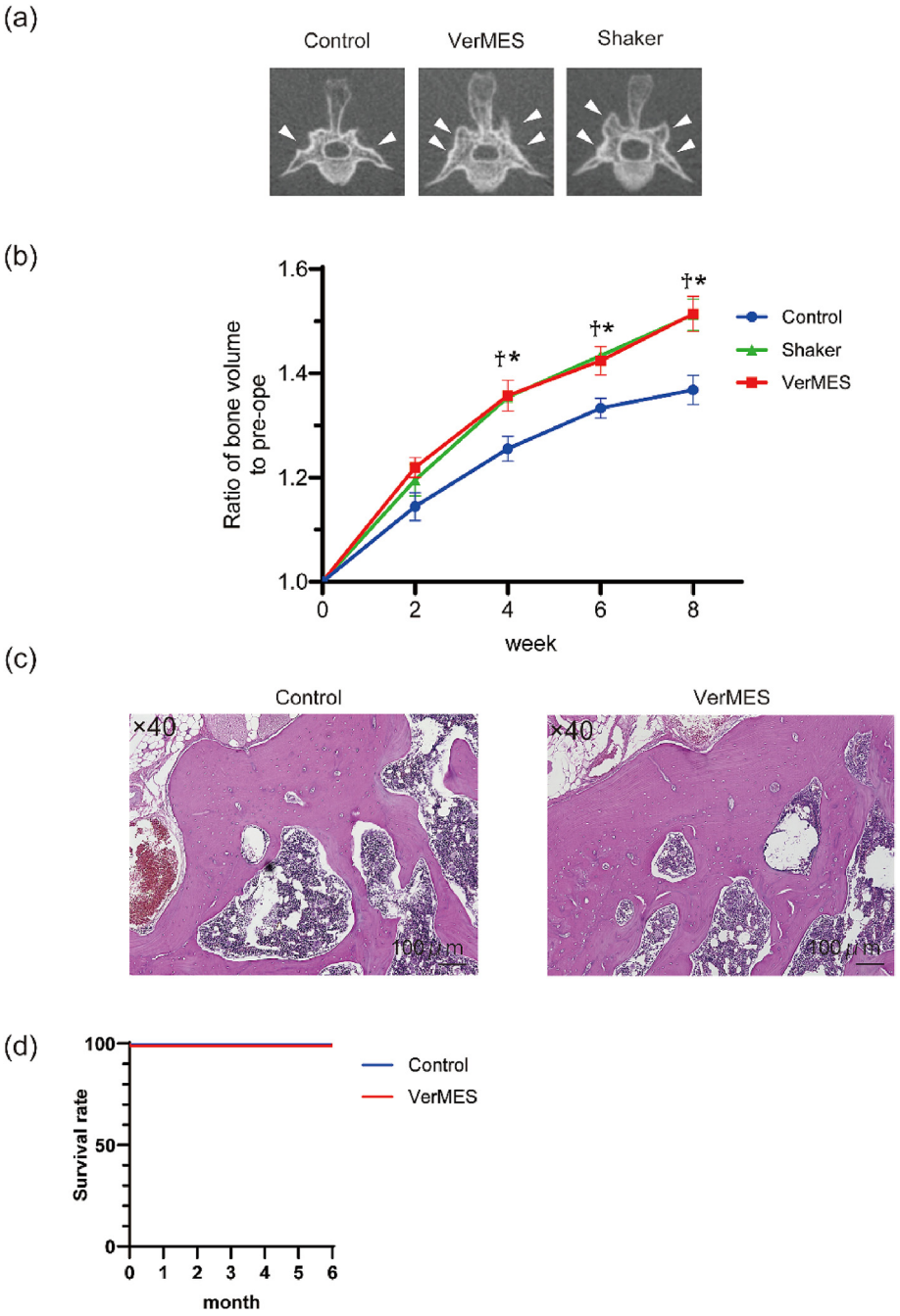

Fig. 2. Rat experiment results

(a) Computed tomography axial images of the rat lumbar spine at 8 weeks after surgery. White arrowheads indicate areas of new bone formation. (b) Graph showing the ratio of bone volume to preoperative bone volume at each time point. The bone volume ratios in the VerMES and shaker groups were significantly larger than those in the control group at 4, 6, and 8 weeks after the operation. No significant differences were observed between the VerMES and shaker groups; *$p < 0.05$ for the comparison between the control and VerMES groups, and $^{\dagger}p < 0.05$ for the comparison between the control and shaker groups. (c) Hematoxylin and eosin-stained images of the spines of the control and VerMES groups at 8 weeks postoperatively. In both groups, the transplanted artificial bone ossified on the existing bone cortex of the vertebral arch, forming a new thick bone cortex. The border with the internal trabecular bone also became unclear, indicating that high-quality remodeling occurred. (d) Survival curves drawn using the Kaplan–Meier method for the occurrence of adverse events in the control and VerMES groups. No adverse events, including death, were observed in either group.

10 ng/mL bFGF [15]. This study revealed that the levels of growth factors in S-FD-iMPs and V-FD-iMPs were not less than those in PRP. Despite the differences in growth factor levels, no significant difference was observed in bone formation in rats between the V-FD-iMP and S-FD-iMP groups. The mechanisms underlying these findings are currently unclear. One hypothesis is that other factors such as extracellular vesicles released from platelets, which are known to be important for tissue repair in PRP [33,34], may have as great an effect on bone formation as the cytokines. However, further research is required to confirm these hypotheses.

Administration of V-FD-iMPs to rats and rabbits had no adverse events, including severe inflammatory reactions and tumor formation at the administration site, suggesting that V-FD-iMPs are safe for animal models. One of the risks associated with using iPS cell-derived preparations is tumorigenesis. However, no live cells remain after freeze-drying treatment. Indeed, no tumor formation

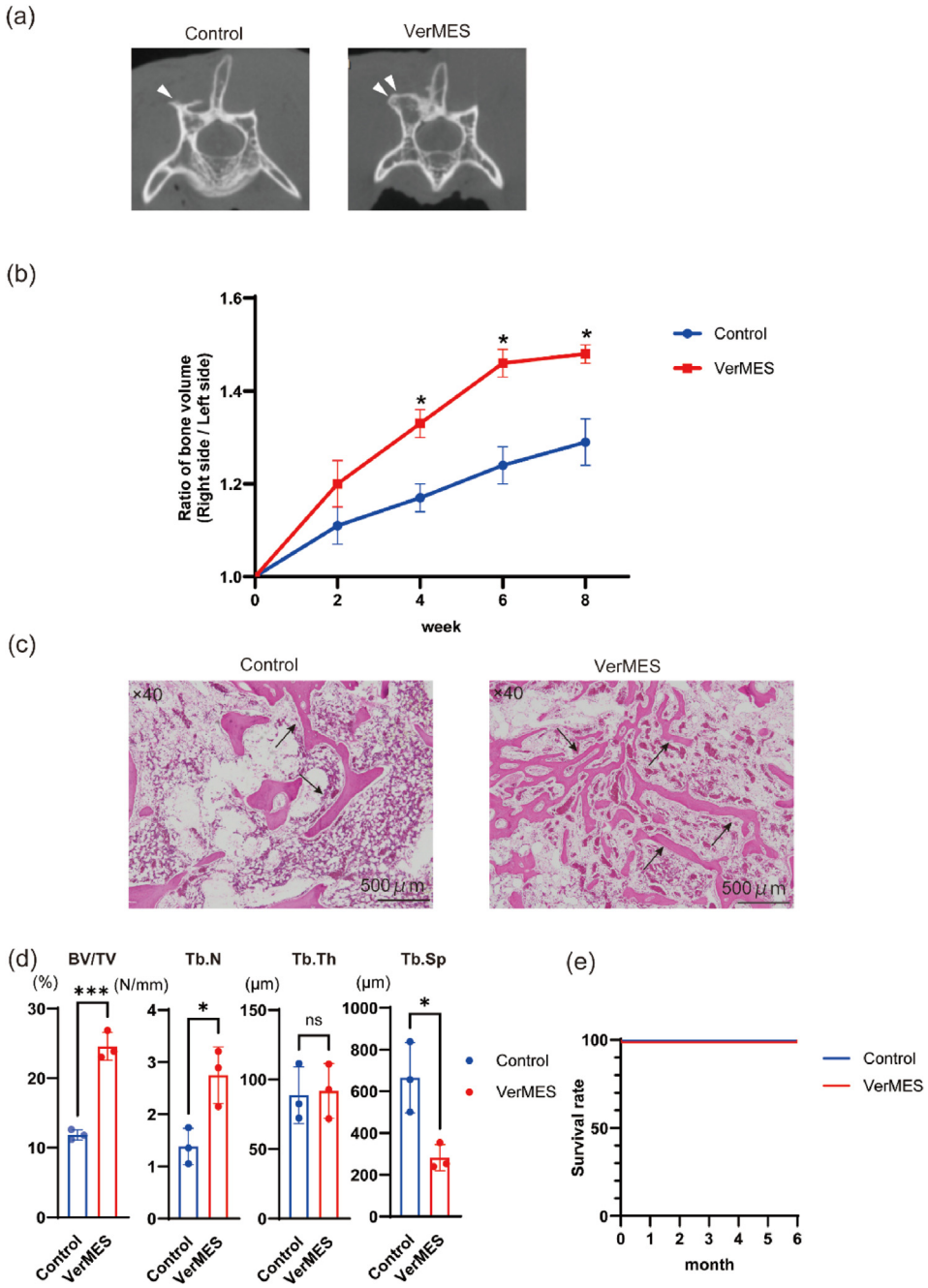

Fig. 3. Rabbit experiment results

(a) Computed tomography axial images of the rabbit lumbar spine at 8 weeks after surgery. White arrowheads indicate areas of new bone formation. (b) Graph showing the ratio of the bone volume of the operated side to that of the non-operated side at each time point. The VerMES group showed significantly greater bone volume ratios than the control group at 4, 6, and 8 weeks after the operation; *$p < 0.05$ for the comparison between the control and VerMES groups. (c) Hematoxylin and eosin-stained images of the new bone formation area in the control and VerMES groups 8 weeks postoperatively. The black arrow shows the typical trabecular bone branches. The VerMES group showed more abundantly formed trabecular bone branches than the control group. (d) BV/TV and Tb.N were significantly higher and Tb.Sp was significantly lower in the VerMES group than in the control group. (e) Survival curves drawn using the Kaplan–Meier method for the occurrence of adverse events in the control and VerMES groups. No adverse events, including death, were observed in either group.

was observed in this experiment. In addition, iPSC-derived platelets can be genetically engineered to lack HLA class I [35], potentially reducing immune reactions. Therefore, we believe that the V-FD-iMP preparation has excellent potential for clinical applications in the future.

One limitation of this study is that bone union and strength should have been evaluated. Our previous study on S-FD-iMPs did not show bone fusion at 8 weeks [22]. Nevertheless, a study with Refit© and rat PRP in a rat anterior lumbar fusion model reported 40 % bone fusion at 8 weeks and 100 % fusion at 12 weeks [36]. We mainly use hydroxyapatite in animal studies because it is easier to manipulate. As for other bone materials, demineralized bone matrix already contains growth factors because it is derived from human bone, and β-tricalcium phosphate is not easily absorbed; therefore, it is difficult to see differences in effect. Hydroxyapatite does not have these disadvantages, but it is easily absorbed and

sometimes does not lead to bone fusion. Therefore, the 8-week assessment in our study may have been too short, and the use of other bone materials could be considered in the future.

The optimal iMP dosage must also be determined. Low platelet concentrations in PRP have been reported to have little effect on bone formation, whereas high platelet concentrations are detrimental to osteoblasts, possibly due to the amount of growth factors present in PRP [37]. As rabbits weigh approximately four times as much as rats, we administered iMPs bilaterally between two vertebrae in rats and unilaterally in one vertebra in rabbits. The difference in local cytokine concentrations may have affected bone formation. Additional studies are necessary to determine the optimal amount needed for osteoblast proliferation and bone differentiation. Furthermore, while this study primarily focused on the efficacy of iMPs, we acknowledge that a direct comparison between the osteogenic effects of human peripheral blood platelets and iMPs has not yet been performed. This comparison is crucial to fully understand the relative bone-promoting abilities of each, and will be an important focus of future investigations.

5. Conclusions

In conclusion, the efficacy of V-FD-iMPs produced on a clinical scale in promoting bone formation in rats was comparable to that of S-FD-iMPs produced on an experimental scale, with no adverse events. Moreover, the V-FD-iMPs significantly promoted bone formation in rabbits without causing adverse events, yielding trabecular bone branches of similar thickness to those of the control group but with a denser construction. These findings suggest that this clinical-scale formulation safely and effectively promotes bone formation.

Resource availability

Data and code availability: The datasets used and analyzed during this study are available from the corresponding author on reasonable request.

Author contributions

Y.S., N.T., M.M., S.T., K.K., M.S., K.I., M.S–N., Y.E., S.Orita, K.E, and S.Ohtori designed and supervised this study. I.T., S.N., H.O., and S.K. instructed and collaborated on the experiments. T.A. managed and conducted this study, performed the statistical analyses, and wrote the manuscript. All authors read and approved the final manuscript.

Declaration of Generative AI and AI-assisted technologies in the writing process

None.

Declaration of competing interest

Y.S., M.M., N.T., K.K., K.E. and S.Ohtori hold stock of Kineplat Co.Ltd. that has a related patent of this research.

Acknowledgments

This study was supported by AMED (Grant Number JP24ym0126136h0001), JSPS KAKENHI (Grant Numbers 19K09615, 22H03193, and 23K15706), TERUMO LIFE SCIENCE FOUNDATION, and ZENKYOREN (National Mutual Insurance Federation of Agricultural Cooperatives.) We thank Editage (www.editage.com) for English language editing.

References

[1] Chen X, Jones IA, Park C, Vangsness CT. The efficacy of platelet-rich plasma on tendon and ligament healing: a systematic review and meta-analysis with bias assessment. Am J Sports Med 2018;46:2020–32. https://doi.org/10.1177/0363546517743746.
[2] Everts P, Onishi K, Jayaram P, Lana JF, Mautner K. Platelet-rich plasma: new performance understandings and therapeutic considerations in 2020. Int J Mol Sci 2020;21:7794. https://doi.org/10.3390/ijms21207794.
[3] Filardo G, Previtali D, Napoli F, Candrian C, Zaffagnini S, Grassi A. PRP Injections for the treatment of knee osteoarthritis: a meta-analysis of randomized controlled trials. Cartilage 2021;13:364S. https://doi.org/10.1177/1947603520931170. 75S.
[4] Sheean AJ, Anz AW, Bradley JP. Platelet-rich plasma: fundamentals and clinical applications. Arthroscopy 2021;37:2732–4. https://doi.org/10.1016/j.arthro.2021.07.003.
[5] Kubota G, Kamoda H, Orita S, Yamauchi K, Sakuma Y, Oikawa Y, et al. Platelet-rich plasma enhances bone union in posterolateral lumbar fusion: a prospective randomized controlled trial. Spine J 2019;19:e34–40. https://doi.org/10.1016/j.spinee.2017.07.167.
[6] Otagiri T, Shiga Y, Hozumi T, Matsuura Y, Tajiri I, Takayama N, et al. Combined effect of DBM, PRP, and bone marrow fluid on bone union in a rat posterolateral fusion model. Sci Rep 2023;13:15041. https://doi.org/10.1038/s41598-023-41844-5.
[7] Van Lieshout EMM, Den Hartog D. Effect of platelet-rich plasma on fracture healing. Injury 2021;52(Supplement 2):S58–66. https://doi.org/10.1016/j.injury.2020.12.005.
[8] Kamoda H, Ohtori S, Ishikawa T, Miyagi M, Arai G, Suzuki M, et al. The effect of platelet-rich plasma on posterolateral lumbar fusion in a rat model. J Bone Joint Surg Am 2013;95:1109–16. https://doi.org/10.2106/JBJS.L.00320.
[9] Li S, Xing F, Luo R, Liu M. Clinical effectiveness of platelet-rich plasma for long-bone delayed union and nonunion: a systematic review and meta-analysis. Front Med 2021;8:771252. https://doi.org/10.3389/fmed.2021.771252.
[10] Simman R, Hoffmann A, Bohinc RJ, Peterson WC, Russ AJ. Role of platelet-rich plasma in acceleration of bone fracture healing. Ann Plast Surg 2008;61:337–44. https://doi.org/10.1097/SAP.0b013e318157a185.
[11] Shiga Y, Orita S, Kubota G, Kamoda H, Yamashita M, Matsuura Y, et al. Freeze-dried platelet-rich plasma accelerates bone union with adequate rigidity in posterolateral lumbar fusion surgery model in rats. Sci Rep 2016;6:36715. https://doi.org/10.1038/srep36715.
[12] Muthu S, Jeyaraman M, Ganie PA, Khanna M. Is platelet-rich plasma effective in enhancing spinal fusion? Systematic overview of overlapping meta-analyses. Global Spine J 2022;12:333–42. https://doi.org/10.1177/2192568220988278.
[13] Peerbooms JC, Colaris JW, Hakkert AA, Van Appeldorn M, Bruijn DJ, Den Oudsten BL, et al. No positive bone healing after using platelet rich plasma in a skeletal defect. An observational prospective cohort study. Int Orthop 2012;36:2113–9. https://doi.org/10.1007/s00264-012-1603-9.
[14] Yu H, Zhou Z, Yu B, Sun T, Tang Q, Jia Y. The efficacy of platelet-rich plasma applicated in spinal fusion surgery: a meta-analysis. Front Surg 2022;9:924753. https://doi.org/10.3389/fsurg.2022.924753.
[15] Taniguchi Y, Yoshioka T, Sugaya H, Gosho M, Aoto K, Kanamori A, et al. Growth factor levels in leukocyte-poor platelet-rich plasma and correlations with donor age, gender, and platelets in the Japanese population. J Exp Orthop 2019;6:4. https://doi.org/10.1186/s40634-019-0175-7.
[16] McCarrel T, Fortier L. Temporal growth factor release from platelet-rich plasma, trehalose lyophilized platelets, and bone marrow aspirate and their effect on tendon and ligament gene expression. J Orthop Res 2009;27:1033–42. https://doi.org/10.1002/jor.20853.
[17] Nakamura S, Takayama N, Hirata S, Seo H, Endo H, Ochi K, et al. Expandable megakaryocyte cell lines enable clinically applicable generation of platelets from human induced pluripotent stem cells. Cell Stem Cell 2014;14:535–48. https://doi.org/10.1016/j.stem.2014.01.011.
[18] Sone M, Nakamura S, Umeda S, Ginya H, Oshima M, Kanashiro MA, et al. Silencing of p53 and CDKN1A establishes sustainable immortalized megakaryocyte progenitor cells from human iPSCs. Stem Cell Rep 2021;16:2861–70. https://doi.org/10.1016/j.stemcr.2021.11.001.
[19] Takayama N, Nishimura S, Nakamura S, Shimizu T, Ohnishi R, Endo H, et al. Transient activation of c-MYC expression is critical for efficient platelet generation from human induced pluripotent stem cells. J Exp Med 2010;207:2817–30. https://doi.org/10.1084/jem.20100844.
[20] Nakatani Y, Agata H, Sumita Y, Koga T, Asahina I. Efficacy of freeze-dried platelet-rich plasma in bone engineering. Arch Oral Biol 2017;73:172–8. https://doi.org/10.1016/j.archoralbio.2016.10.006.
[21] Shiga Y, Kubota G, Orita S, Inage K, Kamoda H, Yamashita M, et al. Freeze-dried human platelet-rich plasma retains activation and growth factor expression after an eight-week preservation period. Asian Spine J 2017;11:329–36. https://doi.org/10.4184/asj.2017.11.3.329.
[22] Sato M, Shiga Y, Takayama N, Sone M, Kosaka K, Motegi I, et al. The effect of megakaryocytes and platelets derived from human-induced pluripotent stem cells on bone formation. Spine Surg Relat Res 2021;5:196–204. https://doi.org/10.22603/ssrr.2020-0226.
[23] Ito Y, Nakamura S, Sugimoto N, Shigemori T, Kato Y, Ohno M, et al. Turbulence activates platelet biogenesis to enable clinical scale ex vivo production. Cell 2018;174:636–648.e18. https://doi.org/10.1016/j.cell.2018.06.011.

[24] Sugimoto N, Kanda J, Nakamura S, Kitano T, Hishizawa M, Kondo T, et al. iPLAT1: the first-in-human clinical trial of iPSC-derived platelets as a phase 1 autologous transfusion study. Blood 2022;140:2398–402. https://doi.org/10.1182/blood.2022017296.
[25] Sugimoto N, Nakamura S, Shimizu S, Shigemasa A, Kanda J, Matsuyama N, et al. Production and nonclinical evaluation of an autologous iPSC–derived platelet product for the iPLAT1 clinical trial. Blood Adv 2022b;6:6056–69. https://doi.org/10.1182/bloodadvances.2022008512.
[26] Kim G, Inage K, Shiga Y, Mukaihata T, Tajiri I, Eguchi Y, et al. Bone union-promoting effect of Romosozumab in a rat posterolateral lumbar fusion model. J Orthop Res 2022;40:2576–85. https://doi.org/10.1002/jor.25287.
[27] Kirihara Y, Takechi M, Kurosaki K, Matsuo H, Kajitani N, Saito Y. Effects of an anesthetic mixture of medetomidine, midazolam, and butorphanol and antagonism by atipamezole in rabbits. Exp Anim 2019;68:443–52. https://doi.org/10.1538/expanim.18-0183.
[28] Liu Z, Zhu Y, Ge R, Zhu J, He X, Yuan X, et al. Combination of bone marrow mesenchymal stem cells sheet and platelet rich plasma for posterolateral lumbar fusion. Oncotarget 2017;8:62298–311. https://doi.org/10.18632/oncotarget.19749.
[29] Van Eps JL, Fernandez-Moure JS, Cabrera FJ, Taraballi F, Paradiso F, Minardi S, et al. Improved posterolateral lumbar spinal fusion using a biomimetic, nanocomposite scaffold augmented by autologous platelet-rich plasma. Front Bioeng Biotechnol 2021;9:622099. https://doi.org/10.3389/fbioe.2021.622099.
[30] Zakaria Z, Seman CNZC, Buyong Z, Sharifudin MA, Zulkifly AH, Khalid KA. Histological evaluation of hydroxyapatite granules with and without platelet-rich plasma versus an autologous bone graft: comparative study of biomaterials used for spinal fusion in a New Zealand white rabbit model. Sultan Qaboos Univ Med J 2016;16:e422–9. https://doi.org/10.18295/squmj.2016.16.04.004.
[31] Hildebrand T, Laib A, Müller R, Dequeker J, Rüegsegger P. Direct three-dimensional morphometric analysis of human cancellous bone: microstructural data from spine, femur, iliac crest, and calcaneus. J Bone Miner Res 1999;14:1167–74. https://doi.org/10.1359/jbmr.1999.14.7.1167.
[32] Parfitt AM, Drezner MK, Glorieux FH, Kanis JA, Malluche H, Meunier PJ, et al. Bone histomorphometry: standardization of nomenclature, symbols, and units. Report of the ASBMR histomorphometry nomenclature committee. J Bone Miner Res 1987;2:595–610. https://doi.org/10.1002/jbmr.5650020617.
[33] Troha K., Vozel Z, Arko M, Bedina Zavec A, Dolinar D, Hočevar M, et al. Autologous platelet and extracellular vesicle-rich plasma as therapeutic fluid: a review. Int J Mol Sci 2023;24:3420. https://doi.org/10.3390/ijms24043420.
[34] Wu J., Piao Y, Liu Q, Yang X. Platelet-rich plasma-derived extracellular vesicles: a superior alternative in regenerative medicine? Cell Prolif 2021;54:e13123. https://doi.org/10.1111/cpr.13123.
[35] Suzuki D., Flahou C, Yoshikawa N, Stirblyte I, Hayashi Y, Sawaguchi A, et al. iPSC-derived platelets depleted of HLA class I are inert to anti-HLA class I and natural killer cell immunity. Stem Cell Rep 2020;14:49–59. https://doi.org/10.1016/j.stemcr.2019.11.011.
[36] Matsubara T, Yamada K, Kanazawa T, Sato K, Yokosuka K, Shiba N. Improved intervertebral bone union in ALIF rat model with porous hydroxyapatite/collagen combined with platelet-rich plasma. Spine J 2023;23:325–35. https://doi.org/10.1016/j.spinee.2022.08.019.
[37] Weibrich G, Hansen T, Kleis W, Buch R, Hitzler WE. Effect of platelet concentration in platelet-rich plasma on peri-implant bone regeneration. Bone 2004;34:665–71. https://doi.org/10.1016/j.bone.2003.12.010.